

1    **Supplementary Information for “Self-Reconfiguring Mod-**  
2    **ular Robotic Boats”**

3

4    Wei Wang<sup>1,†,\*</sup>, Niklas Hagemann<sup>2,\*</sup>, Alejandro Gonzalez-Garcia<sup>3,\*</sup>, Carlo Ratti<sup>4,5</sup>, Daniela Rus<sup>2,†</sup>

5    <sup>1</sup>*Marine Robotics Lab, Department of Mechanical Engineering, College of Engineering, University*

6    of Wisconsin-Madison, Madison, USA

7    <sup>2</sup>*Computer Science and Artificial Intelligence Lab (CSAIL), Massachusetts Institute of Technology,*  
8    *Cambridge, USA*

9    <sup>3</sup>*MECO Research Team, Department of Mechanical Engineering, KU Leuven, Belgium*

10    <sup>4</sup>*Senseable City Laboratory, Massachusetts Institute of Technology, Cambridge, USA*

11    <sup>5</sup>*ABC Department, Politecnico di Milano, Milano, Italia*

12

13

14    \*These authors contributed equally to this work.

15

16    **Supplementary Note 1**

17    Mini Thruster Design

18    Due to the lack of commercially available brushless thrusters of suitable size for the miniature robotic  
19    boats, we design custom mini thrusters, with mechanical details provided in (see Supplementary Fig. 3b).  
20    To facilitate integration and maintenance, we further develop detachable holders for the thrusters (see  
21    Supplementary Fig. 3a). Additionally, to enhance the rotational inertia of the robot and improve yaw con-  
22    trol, we implement a detachable fin, as shown in see Supplementary Fig. 3a.

23    Electronics and Sensors

24    Each *FloatForm* module relies on an onboard embedded computer (Raspberry Pi 4), running Ubuntu  
25    20.04 operating system, and Robot Operating System (ROS). The Raspberry Pi controls the robot's basic  
26    behaviors, communication with other agents, and interactions with a base station. Each robot also in-  
27    cludes an STM32 microcontroller for lower-level control of peripheral hardware. The microcontroller  
28    receives force and latching commands from the Raspberry Pi. It translates these commands into signals  
29    for the Electronic Speed Controllers (ESCs), which drive the thrusters and signals to the micro-servo mo-  
30    tor to actuate the latching mechanism. On the sensing side, a low-cost Adafruit BNO055 IMU provides  
31    angular velocity data, and two Marvelmind acoustic beacons provide position and heading data. Experi-  
32    mental data is logged onto an onboard microSD card. All electronics are connected to a custom printed  
33    circuit board (PCB). An 11.1-V 2650-mAH Li-Po battery provides power for up to 3 hours of runtime and  
34    is placed in the base of the hull for stability. Assembling a module takes around 2 hours: starting with the  
35    assembly of the thrusters, placement of the battery and electronics, wiring, fixation with screws, place-  
36    ment of the latching system, and fixation of the localization beacons on the acrylic cover.

37    Localization

38    Localization of all robots is facilitated using the Marvelmind Navigation System: an off-the-shelf in-

39 door navigation system, designed to provide precise ( $\pm 2$  cm) location data to autonomous robots via mo-  
40 bile ultrasonic beacons. The navigation system consists of a network of stationary beacons interconnected  
41 via a radio interface in a license-free band; two mobile beacons installed on each module to be tracked;  
42 and a modem providing a gateway to the system from a base-station computer. The location of each mo-  
43 bile beacon can be inferred from the propagation delay of ultrasonic pulses (Time-Of-Flight or TOF) be-  
44 tween stationary and mobile beacons using a trilateration algorithm. An Extended Kalman Filter is then  
45 used to provide a more accurate and higher frequency estimation of the robot state (pose and velocity) by  
46 fusing the data from the beacons with values from the onboard IMU. Nonetheless, the localization data  
47 from the robots is naturally noisy due to two main factors. First, the confined water surface causes com-  
48 plex multi-path effects that affect trilateration. Second, the presence of numerous neighbors causes con-  
49 sistent disturbances that further impact trilateration. As a result, incomplete and imperfect representations  
50 may occur during self-reconfiguration behaviors.

51 Each *FloatForm* robot can obtain its neighbor's position at a sampling rate of 50 Hz using a multi-master  
52 communication framework implemented in ROS via Wi-Fi. Although each robot can theoretically know  
53 the position of all its neighbors within our testing area, the communication range during experiments was  
54 artificially limited by actively discarding messages originating outside the desired communication range  
55 (0.5 m in our case). This limited range reduces the communication load between neighbors and allows the  
56 coordination algorithm to be compatible with different sensing or communication strategies, such as infra-  
57 red or cameras.

58 **Supplementary Note 2**

59 Thrust allocation

60 Given that the thrusters used in the robot are incapable of bi-directional motion (they only provide  
61 forward thrust), have a limited rotational speed, and the vehicle is over-actuated, the following procedure

62 is required to allocate the appropriate command into each thruster. First, consider the forces and moments  
63 vector  $\tau = [\tau_u, \tau_v, \tau_r]^T$  and the actuators vector  $f = [f_1, f_2, f_3, f_4]^T$ , where its relationship is:

64  $f = B^+ \tau$  (1)

65 Notice that the Moore-Penrose pseudo-inverse is used since  $B$  is not a square matrix. Nevertheless, this  
66 allows negative values to be sent to each thruster, which would mean reversing the thruster blade's rota-  
67 tion. Then, each desired thruster signal needs to be mapped to ensure a positive command. First, the min-  
68 imum value  $f_l = \min(f)$  is computed. If  $f_l < 0$ , then  $f_i = f_i - f_l$ , with  $i = 1, 2, 3, 4$ .

69 However, the thrust could still be larger than the maximum value  $f_{\max}$ . Likewise, if each thruster is  
70 limited to  $f_{\max}$ , the thrust ratio or direction could be lost, resulting in a different movement than the de-  
71 sired one, i.e., the motion vector would be redirected. Thus, the maximum command is then identified as  
72  $f_h = \max(f)$ . If the maximum command is larger than the maximum allowed thrust,  $f_h > f_{\max}$ , then  $f_i =$   
73  $\frac{f_i f_{\max}}{f_h}$ , which maintains the original motion direction. Nevertheless, this means the rotational velocity may  
74 be diminished given its different performance range compared to linear velocities. Hence, the procedure is  
75 followed again using a new vector  $\hat{f} = Bf$ , where  $\hat{f}_r$  is replaced by the original heading controller  $\tau_r$ .

76 **Supplementary Note 3**

77 Centralized Task assignment algorithm to solve local imperfections

78 For the centralized part of the proposed system, each module is assigned a position from a shape ma-  
79 trix  $G$ . The position assignment is introduced to ensure that a perfect structure is achieved, as the potential  
80 field algorithm can approximate a shape without guarantees to avoid imperfect square lattices. First, the  
81 shape matrix  $G = [g_1, g_2, \dots, g_M]^T$  is composed of goal positions  $g_m \in R^2$ , for  $m = 1, 2, \dots, M$ , where  $M$  is  
82 the total number of goals/robots (assuming the shape is designed with the same number of available goal

83 positions as there are robots). Next, a distance matrix  $D$  is computed using the distance between each  
84 *FloatForm* module's position  $p_k$  and each goal  $g_m$  as

85 
$$D_{k,m} = ||p_k - g_m||^2 \quad (2)$$

86 Then, an assignment matrix  $\Phi$  is considered, where each matrix position is set to 1 if the robot is assigned  
87 to a goal  $m$ , or to 0 if the robot is not assigned to said goal  $m$ . Thus, it results in the following linear as-  
88 signment problem:

89 
$$\sum_{k=1}^M \sum_{m=1}^M \Phi_{k,m} D_{k,m} \quad (3)$$

90 which is solved via the Hungarian algorithm<sup>1</sup>. After each module has received a fixed position, the decen-  
91 tralized position-reference potential field algorithm drives each module to its respective goal.

92 Distributed position-reference algorithm towards perfect assembly

93 At the final stage of the shape formation process, once the task assignment algorithm has assigned  
94 each robot a desired position, a position-reference formation algorithm is employed to bring the swarm  
95 gradually into the correct configuration. Specifically, each robot receives a position reference,  $p_d$ , that  
96 indicates its designated location within the target shape  $G$ . This algorithm is based on the Artificial Poten-  
97 tial Field method and will compute the desired velocities  $[u_d, v_d]^T$  based on the potential force  $F_p$  (Equa-  
98 tion 9 in the Methods section). The repulsive force  $F_r$ , responsible for preventing collisions and maintain-  
99 ing safe spacing between neighboring robots, remains unchanged from Equation 11 in the Methods sec-  
100 tion. However, the attractive force, which pulls each *FloatForm* module toward its assigned goal  $p_d$ , is  
101 defined by a different equation. The attractive force uses the error vector  $e_p = p_d - p$ , *i.e.*, the differ-  
102 ence between the desired position and the robot's current position. Mathematically, the attractive force is  
103 expressed as:

104  $F_{a,p} = k_{a,3} \exp(|| e_p ||) e_p$  (4)

105 where  $k_{a,3}$  is a gain parameter,  $\exp(|| e_p ||)$  is an exponential term that increases with the distance to the  
 106 goal  $p_d$ , and  $e_p$  is the current positional error. Again, the potential field force  $F_p$  is initially calculated in  
 107 the inertial reference frame and then transformed into  $u_d, v_d$  with equation 14 in the Methods section.  
 108 Thus, the surge and sway speed controllers can drive the module to its assigned position  $p_d$ .

109 Collective transport algorithm

110 When the swarm has latched together into a floating structure, the system can perform collective mo-  
 111 tion. In this sense, the assembled structure can hold its position or navigate as a single unit. The collective  
 112 transport algorithm uses a shape matrix  $G_0 = [g_{01}, g_{02}, \dots, g_{0M}]^T$ , where  $g_{0m} = [\Delta_{xm}, \Delta_{ym}]^T$  are the rela-  
 113 tive positions with respect to the shape center, where  $m = 1, 2, \dots, M$ . When the collective structure is  
 114 tasked to move as a unit, a target shape  $G_T(g_{cT}) = [g_{T1} + g_{cT}, g_{T2} + g_{cT}, \dots, g_{TM} + g_{cT}]^T$  is computed  
 115 based on the desired target shape center  $g_{cT} \in R^2$  and the structure desired orientation  $\theta_d$  angle:

116  $g_{Tm} = R(\theta_d)g_{0m}$  (5)

117 where  $R(\theta_d)$  is a rotation matrix dependent on  $\theta_d$ :

118  $R(\theta_d) = \begin{bmatrix} \cos \theta_d & -\sin \theta_d \\ \sin \theta_d & \cos \theta_d \end{bmatrix}$  (6)

119 This computation describes the translation and rotation of the shape matrix  $G_0$  to the desired position and  
 120 orientation of the floating structure. Following the task assignment solution, each robot can receive its  
 121 updated desired position  $p_d$ , and navigate there using the attractive force from Equation 4.

123 **References**

124 1 Kuhn, H. W. The Hungarian Method for the assignment problem. *Nav Res Log* **52**, 7-21 (2005).

125 <https://doi.org/DOI> 10.1002/nav.20053

126

127

128

129

130

131

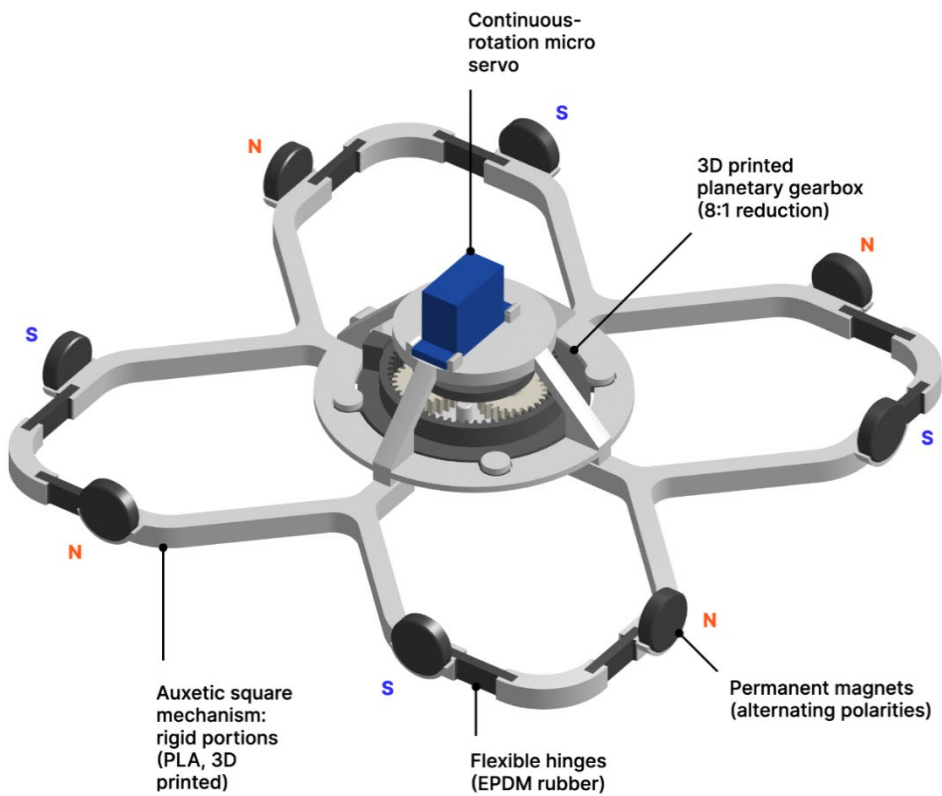
132

133

134

135

136



137

138 **SUPPLEMENTARY FIGURE 1** Mechanical details of the latching mechanism showing the servo  
139 motor, origami-inspired auxetic mechanism, and 3D printed gearbox assembly.

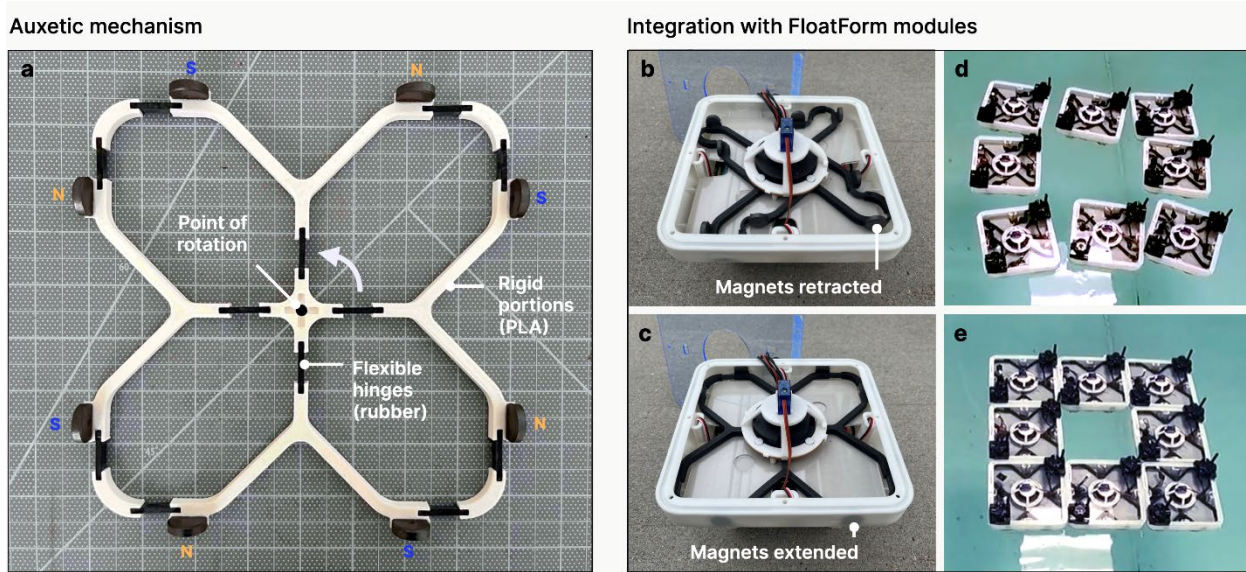
140

141

142

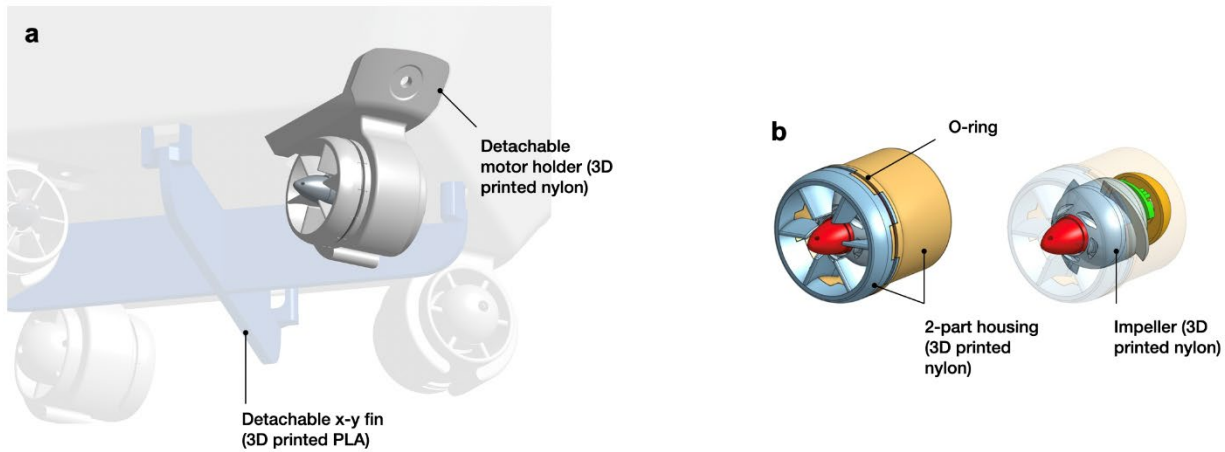
143

144



145  
 146 **SUPPLEMENTARY FIGURE 2. Latching mechanism design.** (a) The auxetic mechanism before as-  
 147 sembly with the motor and gearbox, showing rigid (3D printed PLA) and flexible (EPDM rubber) por-  
 148 tions. Magnets are arranged in an alternating fashion; rotation at the center causes the mechanism to con-  
 149 tract from all sides, bringing the magnets into their retracted (de-latched) positions (b and d). c, and e  
 150 show the mechanism in its latched state.

151  
 152  
 153  
 154  
 155  
 156  
 157  
 158  
 159  
 160  
 161  
 162

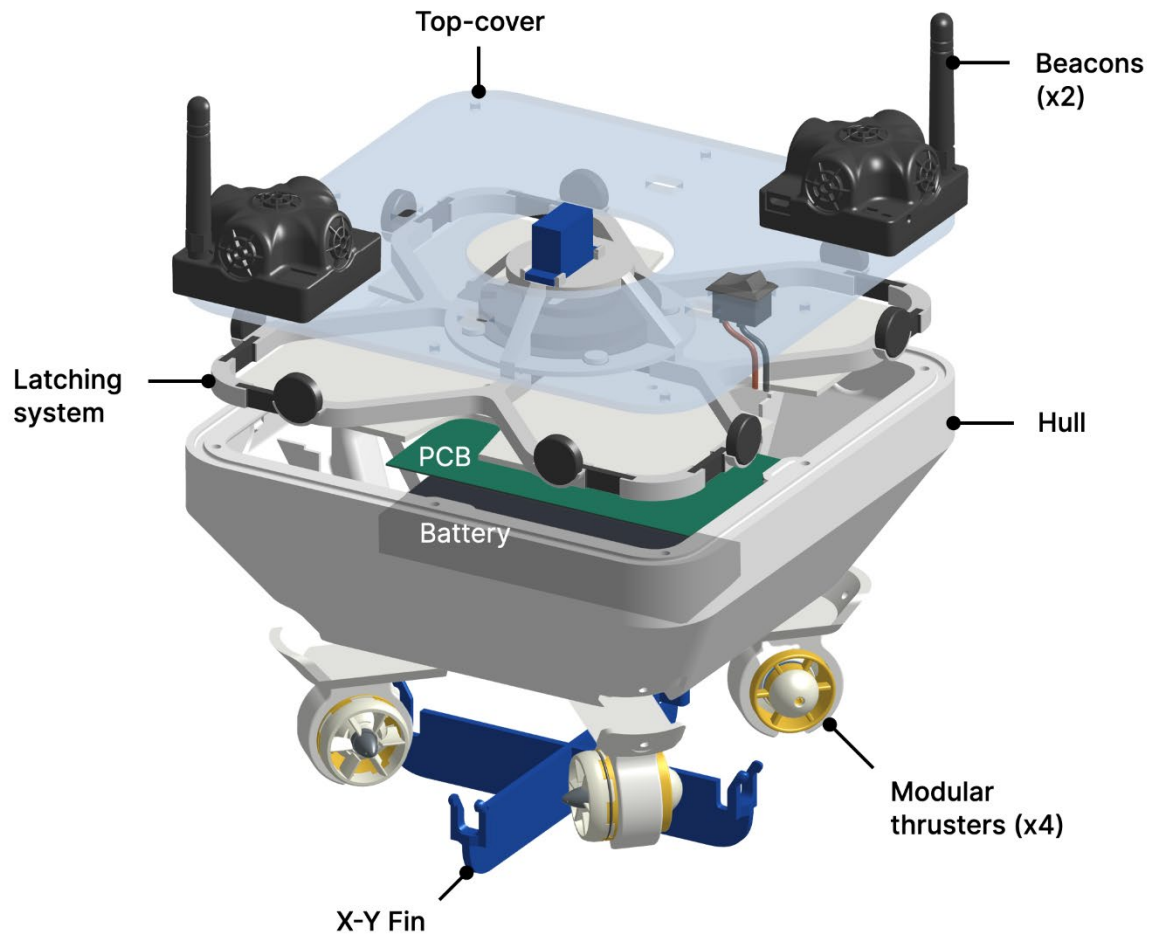


163

164 **SUPPLEMENTARY FIGURE 3 Mechanical details of the robot thrusters:** (a) showing the detachable fin for altering the rotational inertia of the boat and detachable holders for the thrusters, (b) mechanical details of the customized mini thrusters that were developed.

167

168



169

170 **SUPPLEMENTARY FIGURE 4** Exploded view of the robot assembly.

171

172

173

174

175

176

177

178 **Supplementary Video 1: Motion Demonstration**

179 <https://youtu.be/n2NeAlJIIRM>

180 Demonstrates individual module maneuverability in water.

181 **Supplementary Video 2: Latching Mechanism**

182 <https://youtu.be/KXmRcd14U6k>

183 Illustrates the magnetic latching process between modules during docking and undocking.

184 **Supplementary Video 3: Self-Assembly and Reconfiguration with Four Modules**

185 <https://youtu.be/PDxQCSw4xlU>

186 Shows self-assembly and reconfiguration using a small-scale four-module setup.

187 **Supplementary Video 4: Self-Assembly, Reconfiguration, and Collective Transport with**

188 **Eight Modules**

189 <https://youtu.be/DidZ9nz3ax4>

190 Demonstrates self-assembly, reconfiguration and coordinated transport using eight modules.

191

192